Exploiting the interplay between bi-modal molecular weight distribution in polystyrene and humidity to induce self-assembly of biomimetic micropillars/honeycomb morphology in thin polymer film

Authors: Maciej Łojkowski[1,*], Adrian Chlanda[1,2], Emilia Choińska[1], Wojciech Swieszkowski[1*].

Affiliation:

1. Faculty of Material Sciences and Engineering, Warsaw University of Technology, Wołoska 141, 02-507 Warsaw, Poland
2. Department of Chemical Synthesis and Flake Graphene, Łukasiewicz Research Network - Institute of Microelectronics and Photonics, Aleja Lotników 32/46, 02-668 Warsaw, Poland.

Abstract

Segregation of polymer chains of different molecular weights is a well-known process. For many years, it was assumed that this process occurs over long-time intervals. On the contrary, solvent evaporation during spin-coating is very fast. A traditional experimental approach of studying phase segregation of thin films composed of polymer blends with identical chemical compositions but different molecular weights, was focused on functionalization of chemical group or modification of end-group. In this study however, a different approach was proposed, in which polystyrene with a bimodal molecular weight distribution but no additional chemical modification was implemented in order to examine and analyze its phase segregation. By doing this, we have presented an easy, fast, effective and fully controlled method of obtaining biomimetic micropillar/honeycomb morphologies. In addition, the evaporation rate during spin-coating and the viscosity of a solution with a bimodal molecular weight distribution was described.

Keywords

self-assembly; polymer thin films; bimodal molecular weight distribution; polystyrene; spin-coating; pillars; honeycomb;

Introduction

Biomimetic complex morphologies compromising micropillars have gained attention due to their wide range of possible applications, for example, their special wetting properties (1,2), application in studying of biofilm formation (3) or controlling stem cells differentiation (4). Two widespread methods which allow creation of a broad range of structures of polymer thin films (PTFs) are spin-coating (5) and breath figures (6). These methods were applied for manufacturing organic ferroelectric switches (7), light emitting devices (8), sensors (9,10), drug delivery systems (11,12), biologically active surfaces (13,14), functional nanostructured surfaces (15,16), and membranes (17). Both these processes rely heavily on the interaction dynamics between the solvent, the polymer and the vapors in the vicinity of the surface. In the case of spin-coating, a droplet of a mixture of a solvent and one or two polymers is dropped onto the substrate and subsequently the substrate is rotated very quickly to cover it uniformly with the liquid film of the solution. As a result, the solvent evaporates thus a solvent and temperature quench occurs. The change of the solvent volume and temperature often leads to unintentional or intentional liquid-liquid phase separation. (18) It has been argued that such phase separation often starts in the early stages of spinning. (18,19) The further spinning of the solution leads to gel formation which eventually slows down the diffusion inside the film. As a result, he occurring morphology becomes frozen in time before reaching an equilibrium. The time necessary for the morphology to stop evolving depended on such factors as the solvent evaporation rate, solution viscosity or spinning rate. (20,21) In case of the second aforementioned technique, the breath figures appear on the surface of the liquid film when the

humid air flow accelerates the evaporation rate. Successively, the temperature decreases which results in nucleation and growth of water droplets. These droplets create the regular a honeycomb array of cavities in the film. After most of the solvent had evaporated the temperature increases to that of the surroundings, the droplets evaporate leaving a porous surface. The start of the nucleation of these droplets is governed by the onset time related to the solvent evaporation rate, solution concentration and air flow.(22)

The factors which regulate the final morphology, like the solvent type (23), concentration(24), the spinning rate (21) and blend composition (25,26), were already intensively studied. However, the effect of molecular weight distribution (MWD) is still not well understood. Regarding the subject of the PTFs, scientific literature focuses mostly at the polymers with narrow MWD. Conversely, Wu et al. have studied the effect of MWD on the self-assembly of end-functionalized polystyrenes. They proposed a new way of controlling the morphology of PTF obtained via breath figures by changing the MWD width. As result the porous membrane with a higher robustness was obtained.(27)

Thus, it should be highlighted that the location and the width of the MWD can affect polymer solution properties and, as a result, solid thin polymeric films formation. The width of the MWD can be tailored either within the polymerization process (28,29) or by mixing two polymer species with very narrow MWD (30). By tailoring the concentration and location of the two nodes of the distribution of a bimodal polymer, it is possible achieve properties that are otherwise unavailable.(31) As an example, Heitmiller et al. have reported that the heterogeneous melt of polyethylene had higher flow index than the homogeneous one.(32) The investigation performed by the Koningsveld et al. have shown that the bimodal MWD has got a significant effect on the liquid-liquid binodal curve of polymers in solution. (33) Such a solution is characterized by phase regions and liquid-liquid phase separation between polymer- and solvent- rich fractions can occur. Zeman et al. have demonstrated that the critical

concentration enabling phase separation in a solution of two polymer species, decreases with an increase in the molecular weight M_w.(34) Moreover, even when the polymer – polymer interactions are athermal, i.e. Flory-Huggins interaction parameter χ equals zero, the phase separation can occur due to the large difference in entropy between long and short chains, which in fact act as separate entities.(35) This impacts the viscosity of bimodal solutions. Harris et al. have found that the viscosity of the blend of bimodal polystyrene can be considered as a sum of components.(36) It has been discussed that blending polystyrenes with different molecular weight mixed the entanglement types between polymer chains. Furthermore, it was presented that the concentration of the polymers in the solvent changes how the polymer chains interact. It was found that two polymer chains, with the same monomer chemical structure, would act as two different polymers, provided that the concentration is below the overlap concentration (C*). However, once the overlap concentration occurs, the cooperative motion of the polymer starts and the behavior of the solution changes. (37,38)

Successive research focused on studying how the polymer chains of varying lengths segregate in PTF. Hariharan et al. investigated the effect of the entropy of spin-coated and annealed bimodal PTF on polymer chain segregation.(39) It was shown that higher entropy of shorter chains led to their segregation on the PTF surface, while the lower entropy of the longer chains promoted their segregation in the bulk. Tanaka et al. in turn studied spin-coated polystyrenes blends with low and high M_w with narrow MWD utilizing toluene as a solvent. They reported that the PTFs consisting of polystyrenes with a low molecular weight demonstrated surface segregation after thermal treatment.(30) Several other recent studies have illustrated segregation of lower molecular mass elements towards the surface during annealing.(40–44)

On the other hand, it has been shown that segregation of the deuterated polymer can change the surface roughness after having annealed the coating.(45–48)

Despite the extensive studies performed on bimodal polymer solutions and melts, the segregation during short time scales, for example during spin-coating, when the solid polymer film is established within few seconds, was not observed until now for pristine polystyrene. In addition, there is a scarcity of data on spin-coating of polystyrene (PS) in the system with methyl ethyl ketone (MEK), though MEK is considered to be a marginal solvent for PS.(49,50) Though, MEK is good choice as a solvent, it is more hydroscopic then typically used solvents for polystyrene. Thus, it can by a good choice for spin-coating under high humidity conditions. This article discusses the phase segregation of the low and high molecular weight fractions of the polystyrene with bimodal MWD dissolved in MEK. The humidity level during the spin coating process was precisely controlled and spin-coating at humidity ranging up to 75% was performed. By combining entropic interactions between longer and shorter polymer chains and interfacial tension between the polymer solution and condensing water from moist air, it was shown that this conditions leads to a complex morphology consisting of a honeycomb filled with micropillars.

Additionally, the local mechanical properties of the coatings using atomic force microscopy were examined. The viscosity parameters of the bimodal blends were tabularized, and the solubility of the low and high molecular weight polystyrene was discussed.

2. Experimental

2.1 Materials

All polymers and solvents were purchased from Sigma Aldrich (Merck KGaA). One side polished ultra-smooth SiOx wafers were bought from Technolutions Sp. z o. o.

2.2 Preparation of the coatings

Analytic standard grade polystyrenes (PS) as obtained from the supplier with PDI = 1.04 and M_w = 20 kDa, 91 kDa, 150 kDa or 200 kDa, were used.

Two kinds of blends were prepared: the blends of 20 kDa and 200 kDa PS mixed in 75/25, 50/50, 25/75 w/w % proportions; alike the blends of 91 kDa and 200 kDa PS mixed in the same proportions. The as prepared PS solutions were being mixed in methyl ethyl ketone (analytic grade, MEK), for an hour at 37 ^{O}C. After mixing, the solutions were stored overnight. The list of polystyrene blends used is summarized in the Table 1. The concentrations of these solution ranged from 2.5 mg/ml to 80 mg/ml. Solutions were spin-coated onto a silicon wafers under low relative humidity (Rh ~ 0%). DIY Arduino based spin-coater with a chamber with controlled humidity was used to spin polystyrene films onto the SiOx wafers. The experimental setup is depicted in Supplementary Information (SI) Fig. S1 – S2. A 35 µl of the solution was pipetted on the 1 cm x 1 cm wafer. The spin-coating was performed in a closed chamber with a constant air flow of 10 ml/min of dry air to maintain the desired humidity. The rotational speed was 2700 rpm. The spinning time was set to 10 s to allow the solvent to evaporate.

For spin-coating in moist atmosphere the relative humidity was changed to 45%, 55% or 75%. Again 35 µl of the solution (80 mg/ml) was pipetted on the 1 cm x 1 cm wafer and then accelerated to 3300 RPM.

Table 1. List of polymer blends that were used for spin-coating.

Type of Blend	**Sample code**	**Molecular weight M_w [kDa]**		**PDI**
Uniform	20 kDa	20		1.04
	91 kDa	91		1.04
	150 kDa	150		1.04
	200 kDa	200		1.04
Bimodal	**Sample code**	**Molecular weight**		**PDI**
		[M_w] [kDa] (1	**[M_n] [kDa] (2**	

91 kDa / 200 kDa	75/25*	137	118	1.16
	50/50*	166	146	1.14
	25/75*	186	173	1.08
20 kDa / 200 kDa	75/25**	158	65	2.43
	50/50**	184	110	1.67
	25/75**	194	155	1.25

[1]Weight average molecular weight $[M_w] = (f_1M_{w1}^2 + f_2M_{w2}^2)/ (f_1M_{w1} + f_2M_{w2})$, *[2]Number average molecular weight* $[M_n] = f_1M_{w1} + f_2M_{w2}$, *where f - fraction of one of the polymers in %; PDI states for the Polydispersity index.*

Additionally, two blends: 1) 20 kDa and 200 kDa polystyrene (75/25**) and polymethyl methacrylate (PMMA, 20 kDa, 1.04 PDI, Sigma Aldrich, polymer standard grade), 7:3 ratio of bimodal PS to PMMA; 2) 20 kDa and 200 kDa polystyrene (75/25**) and polyvinylpyrrolidone (PVP, 29 kDa average, Sigma Aldrich), 7:3 ratio of bimodal PS to PVP; were used.

2.3 Gel permeation chromatography (GPC)

The number and weight average molecular weights (M_n and M_w) were determined by a modular system Agilent 1200 series GPC with a refractive index detector (RID) equipped with two PLgel 5 µm MIXED-C columns (300x7.5 mm) in the series, while polydispersity index was calculated as the ratio of M_w/M_n. Calibration was performed using a set of 12 narrow-distributed polystyrene standards with the molecular weight (M_p) in the range of 474 g/mol - 1 800 000 g/mol.

The measurements were performed at 35 °C, the chloroform GPC grade was used as a solvent at the flow rate of 0.7 ml/min. All samples (~2 mg/ml) were filtered through PTFE 0.2 µm membrane before the analysis. The data were collected by ChemStation for LC and analyzed by ChemStation GPC Data Analysis Software.

2.4 Force Spectroscopy FS and Elastic Modulus

When a Force Spectroscopy experiment is performed, an AFM probe applies strain on the film surface. During the process a force/displacement curve is gathered. (51) Force spectroscopy was performed by means of the atomic force microscope (AFM, Asylum Research MFP3D Bio). (52) OMLCT-AC200TS-R3 (Olympus) cantilever was used with the nominal spring constant k = 9 N/m and the tip radius below 10 nm as suggested by the cantilever's producer. AFM was calibrated using built-in thermal vibrations method. (53) In order to calculate the elastic modulus (E) from the obtained force/displacement curves a Johnson, Kendall and Roberts (JKR) model was applied. (54) The indentation depth was ~8 nm (Supplementary Information, *4. Force Spectroscopy*). As we wanted to neglect the possible influence of stiff (silica) substrate on registered mechanical data of the polystyrene coating, we decided to perform FS experiment using the thickest films (films spun from solution of concentration of 80 mg/ml).

Maps of large area of the coating 80 μm x 80 μm with resolution 40 x 40 points were obtained. These higher resolution maps are supplemented as an attachment (SI). These data were supported by lower resolution maps with the resolution 15 x 15 points. Each map was used to obtain the mean elastic modulus value. Altogether, at least 5 maps were made. Ordinary one-way ANOVA followed by multiple comparisons Fisher's test was used to compare the means between different groups.

Furthermore, histograms representing each higher resolution map were prepared. Skewness of the elastic modulus distribution was measured. Skewness was divided into two groups: one for the uniform coatings and one for bimodal coatings. The t test ($p < 0.05$) was used to compare between the means of these two groups.

2.5 Evaluation of thickness of spin-coated films by means of atomic force microscopy

To assess the thickness of the coatings some area was scratched off. The thickness of spin-coated films was assessed based on the topography images of the scratch, recorded using the atomic force microscopy technique as shown in SI Fig. S3. Five randomly selected areas of each sample were tested, and profiles were generated. To avoid any unwanted artefacts, influence on the profiles, each profile line for analysis was averaged from three contiguous lines.

2.6. Imaging of the coatings

The light inverted microscopes (Nikon EPIPHOT 200 and Zeiss Axio Observer) were used for imaging. The atomic force microscope (AFM, Asylum Research MFP3D Bio) working in the tapping mode (AC mode) was used to illustrate the phase composition and topography of the polystyrene films.

2.7 In-situ measurement of evaporation during spin-coating by means of laser light reflectometry with stroboscopic effect

To investigate the thinning of the solution layer while spinning, the in-situ stroboscopic laser light reflectometry was used. The laser light is reflected from the coating during the spin-coating process. The occurring interference pattern can be used to estimate the thinning rate of the solution. (55–57) At the same time, the variability of the amplitude of the degree of reflection ϱ can be used to characterize the emergence of the interfacial instabilities in the coating and roughening of the surface when the coating is spun. (58) The experimental setup is described in SI, Fig. S1 – S2.

Depending on the thickness of the layer, constructive or destructive interreference can occur. The condition for the constructive interference was calculated from Bragg's law: $2n\Delta hcos\theta = m\lambda$, where n is the refractive index of the layer, Δh is thickness of the layer, θ – incident angle,

214 m is an integer number and λ is light wavelength. For pure MEK Δh = 235 nm (assuming the
215 refractive index n_{MEK} = 1.3788). For the polymer solution it was assumed that the refractive
216 index was n = 1.5, thus Δh = 217 nm. Laser light wavelength was λ = 650 nm.
217
218 **2.8 Data analysis and visualization**
219 For data visualization and analysis GraphPad Prism 8 was used. For image analysis procedures
220 implemented in Gwyddion software (ver 2.50) were used.
221
222 **2.9 Fourier Transform IR**
223 To determine the functional groups in the films, infrared spectra were collected using a Fourier
224 transform infrared spectrophotometer (Nicolet 8700 FTIR, Thermo Scientific). Measurements
225 were performed using the FTIR ATR over a range of 4000−400 cm−1.
226
227 **2.10 Contact Angle and Surface Free Energy Measurement**
228 The contact angle (CA) was measured using a Data Physics OCA 20 goniometer. The contact
229 angle was measured with a sessile drop method. For Surface Free Energy measurement (SFE)
230 two kinds of coatings were chosen: 20 kDa and 200 kDa. For each type of coating 3 droplets
231 were measured and 3 different coatings were used. Two liquid system was used: deionized
232 water and diiodomethane (Sigma Aldrich, Analytic grade). The groups were compared with t
233 test ($p < 0.05$). Owens, Wendt, Rabel and Kaelble (OWKR) method was used for SFE
234 calculation. (59)
235
236 **3. Result and discussion**

Spin-coating is often described in the literature as a two-step process. (21,57) First, a polymeric solution is dropped on a substrate and spread by the inertia of the rotating substrate (so called flow regime). Subsequently, the solvent evaporates leaving a solid coating.

Notably, manipulating the position of the two nodes in the bimodal MWD can significantly alter the nature of polymer - polymer interactions in the solution in a controllable manner, thus, influencing the solution viscosity. In the research the solutions with bimodal MWD were prepared so that the two nodes in the distribution were clearly separated. The GPC molecular weight distribution of a single node MWD (uniform) is presented in Fig. 1 A, which illustrates the MWD of 91 kDa polystyrene with narrow distribution (PDI=1.04), whereas Fig. 1 B illustrates the MWD with two nodes of a blend of 91 kDa PS with 200 kDa PS, both with narrow distributions (PDI=1.04). GPC investigation confirmed that the molecular weight and MWD of each of the component was the same before and after blending.

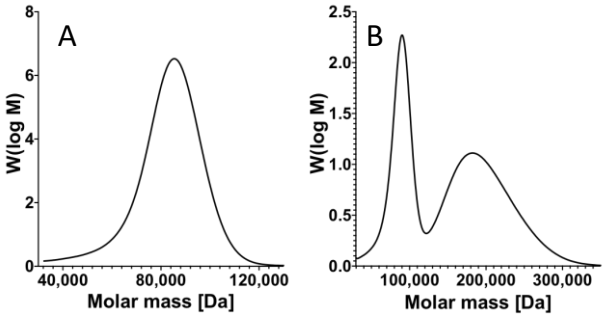

Fig 1. Exemplary GPC experiment results of bimodal and uniform MWD polystyrene; A - narrow uniform MWD, Mw = 91 kDa, PDI 1.04; B – bimodal MWD, blend of Mw = 91 kDa, PDI = 1.04 and Mw = 200 kDa, PDI = 1.04.

The evaporation of the solvent through the spin-coating increased the viscosity of the solution. Successively, the solution concentration fell below the threshold at which the components cannot coexistence as a one phase (Fig 2A and 2B). The arrows mark the paths of the evaporation of the 3 tested compositions: 75/25 w/w%, 50/50 and 25/75, respectively. Due to

the dissimilarity of the molecular weight of lighter and heavier elements the phase diagram is not symmetrical but is shifted towards the lower miscibility of the heavier element.(60)

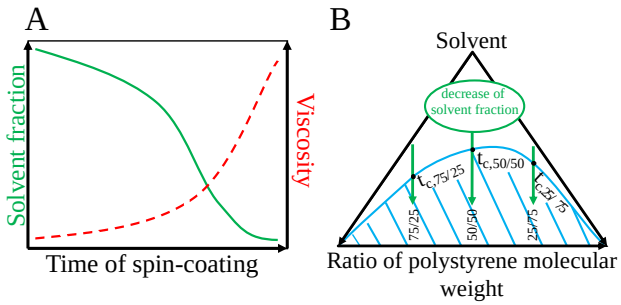

Fig. 2 A – Schematic illustration of the change of the solvent fraction and the solution viscosity due to the evaporation of the solvent during spin-coating; B – Schematic phase diagram in ternary system of polystyrene blend with two molecular weights and solvent. The blue line separates the coexistence region from spinodal decomposition region, illustrated by parallel lines. The arrows illustrate the path of the system as the solvent evaporates with time, t_c is the time necessary to reach a critical concentration at which two phase region exists. 75/25, 50/50, 25/75 – different evaporation paths for the aforementioned polystyrene fractions.

3.1 Evaluation of solution viscosities

The viscosity measurement (Fig. 3.) can be used to assess not only the final coating thickness and the solution evaporation time prediction, but also it can provide information about the character of polymer chains interactions. The measurement result is presented as reduced viscosity η_r/c, where c represents concentration in mg/ml. Here $\eta_r = \frac{\eta - \eta_s}{\eta_s}$, where η is dynamic viscosity of the solution and η_s is the viscosity of the solvent. In Fig. 3A the viscosity is plotted as a function of the concentration.

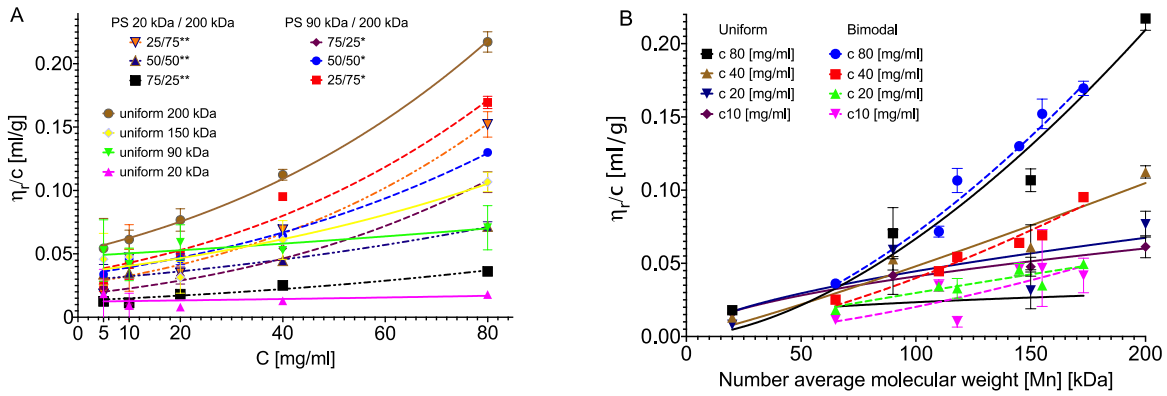

Fig. 3. Reduced viscosity η_r/c of the solutions, A - plotted against the concentration of the solution, B in the function of the number average molecular weight, $[M_n] = f_1 M_{w1} + f_2 M_{w2}$, where f is w/w % ratio of polymers.

The general dependence of viscosity on concentration can be described in a form of a power series:(61)

$$\frac{\eta_r}{c} = [\eta](1 + K[\eta]C + \frac{K[\eta]C^2}{2} + \frac{K[\eta]C^3}{6}) \quad (2)$$

where $[\eta]$ is intrinsic viscosity at infinite dilution. The coefficients are summarized in Table S1 in SI. The difference between bimodal and uniform solution is clearly visible for concentrations surpassing the overlap concentration at around 20 mg/ml.(62) It should be noted that the viscosity of the bimodal solutions increased faster with the increase of the concentration than in case of uniform solutions.

Thereafter Fig. 3B presents the viscosity in relation to the number molecular weight $[M_n]$. The relation between viscosity and molecular weight can be described in a form of the Mark-Houwink equation:(61)

$$\frac{\eta_r}{c} = \ln K + a \ln[M_n]. \quad (3)$$

The K and a coefficient values are summarized in SI, Table S2. Again, a variation between the behavior of uniform and bimodal solutions was registered, while the uniform solutions were visibly more viscous than the bimodal counterpart of similar molecular weight. The positive

solvent – polymer interaction causes swelling of polymer chains, which is further reflected in the enhanced viscosity of polymeric solution. In such case the interactions between polymer chains are more probable. Inversely, the addition of a higher molecular fraction reduces the solubility of the polymer. However, for 80 mg/ml the difference disappeared and the viscosity – molecular weight curves displayed by similar tendencies.

In conclusion, the bimodal solution ware less viscus than the uniform ones at low concentrations ($c < 20$ mg/ml). However, the viscosity in the case of the bimodal blends rapidly increased with the increase of the concentration.

3.2 Evaporation of the solvent during spin-coating

Subsequently, the relation between the viscosity (concentrations c: 20 mg/ml, 40 mg/ml and 80 mg/ml) of the uniform and bimodal solutions and the evaporation rate of the solutions during spin-coating was analyzed (Fig. 4).

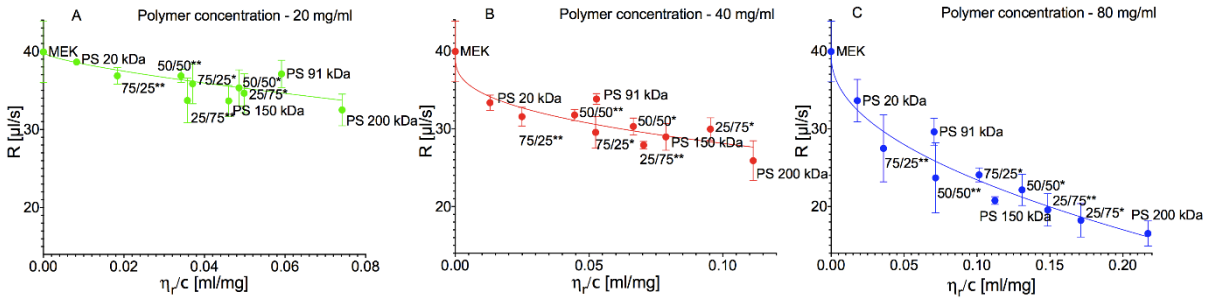

Fig. 4. Relation between the evaporation rate of solution and the reduced viscosity of solution for polymer concentrations: A - 20 mg/ml, B - 40 mg/ml and C - 80 mg/ml, respectively.

Let us now expand the topic of bimodal MWD solution evaporation and compare it with evaporation rate of the solution with the homogeneous MWD. The thinning rate is important, as it allows to extract the height – time profile and predict the evaporation rate and heat behavior

320 at particular time. Especially, the start of the water droplet condensation coming from humidity
321 depends on the temperature fluctuations which are related to the evaporation rate.
322 Evaporation of the solutions was measured by laser reflectometry. The intensity of scattered
323 light increases with solution density, and for higher concentrations clear interference fringes
324 are hard to obtain. This led to choosing solutions with concentration of exclusively 20 mg/ml
325 (which is in proximity to the overlap concentration C*) for further investigation.
326 Fig. 5A presents the first second of solution evaporation in a form of a heat map. The heat map
327 graph (Fig. 5A) presents the thinning rate of the solution ($\Delta h/\Delta t$) in μm/s, where color of each
328 pixel corresponds to the thinning rate value. After 1s the thickness of the film decreased enough
329 for interference to cease. As predicted, the shortest time of this phenomenon was registered for
330 pure MEK. The measured times increased accordingly to the average molecular weight of the
331 solution. In case of solutions with added higher molecular weight fraction after turbulent 0.3 s,
332 a clear region of a slower thinning was found. The region spans between 0.3 s and 0.4 s. Fig.
333 5B presents the evaporation curve of 50/50 w/w % 91 kDa and 200 kDa solution. Subsequently,
334 the region of a lowered thinning rate is followed by a region of an increased thinning rate, which
335 is shifted further in time and prolonged for all solutions with an added fraction of higher
336 molecular weight. It can be assumed, that this phenomenon can be assigned to liquid-liquid
337 phase separation on solvent and polymer rich fraction. It is also possible, that addition of the
338 longer chains facilitates this phase behavior. Then, the behavior of the bimodal solutions would
339 be a mix of properties of its components. On the other hand, this phenomenon can be associated
340 with the final morphology formation. If so, the morphology would start to form in a relatively
341 early stage of the process. Moreover, it can be assumed that the acceleration of evaporation in
342 the later stage would be responsible for the decrease of surface temperature. This will
343 subsequently facilitate water condensation.
344

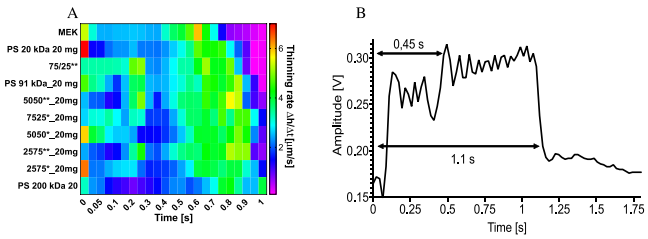

Fig. 5. A - Heat map of the thinning rate of the solution during the spin-coating for concentration of 20 mg/ml; B – representative evaporation curve of 50/50 w/w % 91 kDa and 200 kDa solution, concentration 20 mg/ml, vertical axis corresponds to the voltege amplitude found on the photodetector and the horizontal axis corresponds to the duration of spin-coating.

3.3 Investigation of the thickness and morphology of the coatings spun at Rh 0%

The convection Marangoni flow, solvent evaporation, as well as the phase separation events were found to alter the morphology of the coating surface. As a result, occurrence of wrinkles or arrays of islands on the surface of the coating was reported. (47,63–65)

To determine the effect of bimodal MWD on coating's morphology, the coatings were investigated via AFM and optical imaging. Significant differences between blend types occurred when the solution concentration was 80 mg/ml (Fig. 6A). As illustrated in Fig. 6B the thickness of the coatings in case of 80 mg/ml scaled linearly with the average molecular weight of the blends.

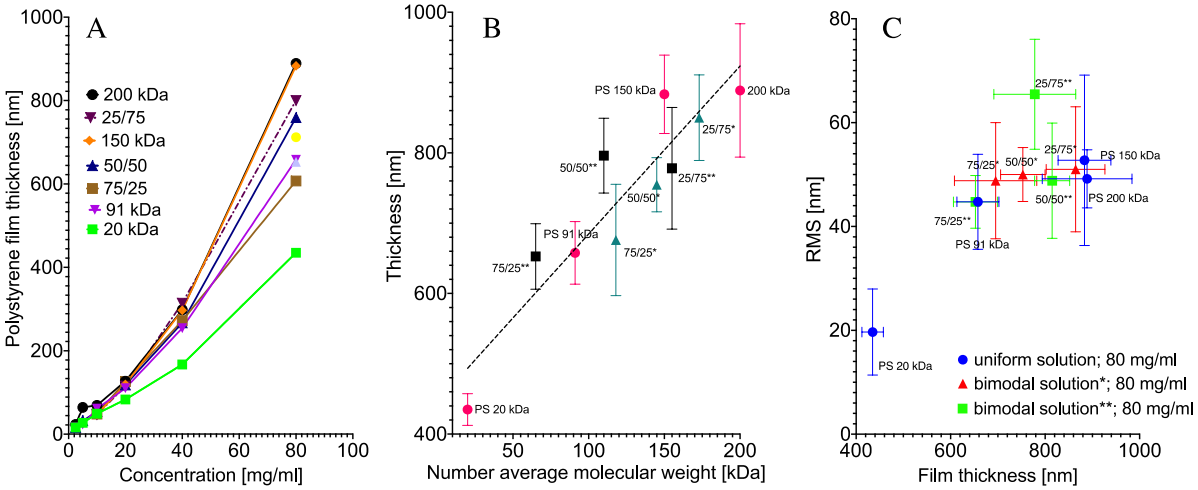

Fig. 6. A - Thickness of the coatings in respect of the composition and the concentration. The plot presents data for uniform and 91 kDa / 200 kDa solutions. B – Thickness of the coating for the concentration of 80 mg/ml in function of the blend's molecular weight. * - Blends of 91 kDa and 200 kDa polystyrene; ** - blend of 20 kDa and 200 kDa polystyrene; x/x – w/w% ratio of blended homogeneous polystyrenes. The number average molecular weight [M_n] = $f_1 M_{w1}$ + $f_2 M_{w2}$, where f w/w. % ratio of polymers. C - RMS roughness of the coatings spun from 80 mg/ml concentration.

In addition it was observed that roughness scales with the film's thickness, the values are not significantly different (Fig. 6C). Nonetheless, the similar RMS value can describe an infinite number of possible morphologies. In order to represent the morphology of the material quantitatively one can apply the Minkowski parameters.(66)

The images (Fig. 7A) used for analysis come from the central part of the image, in order to exclude the high shear rate effect on the coating's morphology. On the basis of this description, it can be concluded that the morphology of the uniform coatings is characterized by separate islands (red color in Fig. 7A) surrounded by a bicontinuous green phase. Oppositely, the bimodal coatings are characterized by a red bicontinuous phase with separate green islands

included. The bicontinuous phase in such case becomes fainter with the increase of the higher weight molecular fraction. This occurrence was observed in case of both kinds of bimodal blends: 20 kDa / 200 kDa and 91 kDa / 200 kDa.

Fig. 7B presents boundary and connectivity. The first of the two parameters, boundary $B(\nu)$ characterizes the number of bound pixels at the edge between dark and bright regions in a binarized picture at a specific threshold ν. Connectivity $C(\nu)$ can be used to describe the bicontinuous or island morphology of the coating in respect to the given binarization threshold ν. The negative value of connectivity corresponds to bicontinuous morphology, while the positive value corresponds to island morphology. Together, those two parameters provide a relevant description of the surface morphology.

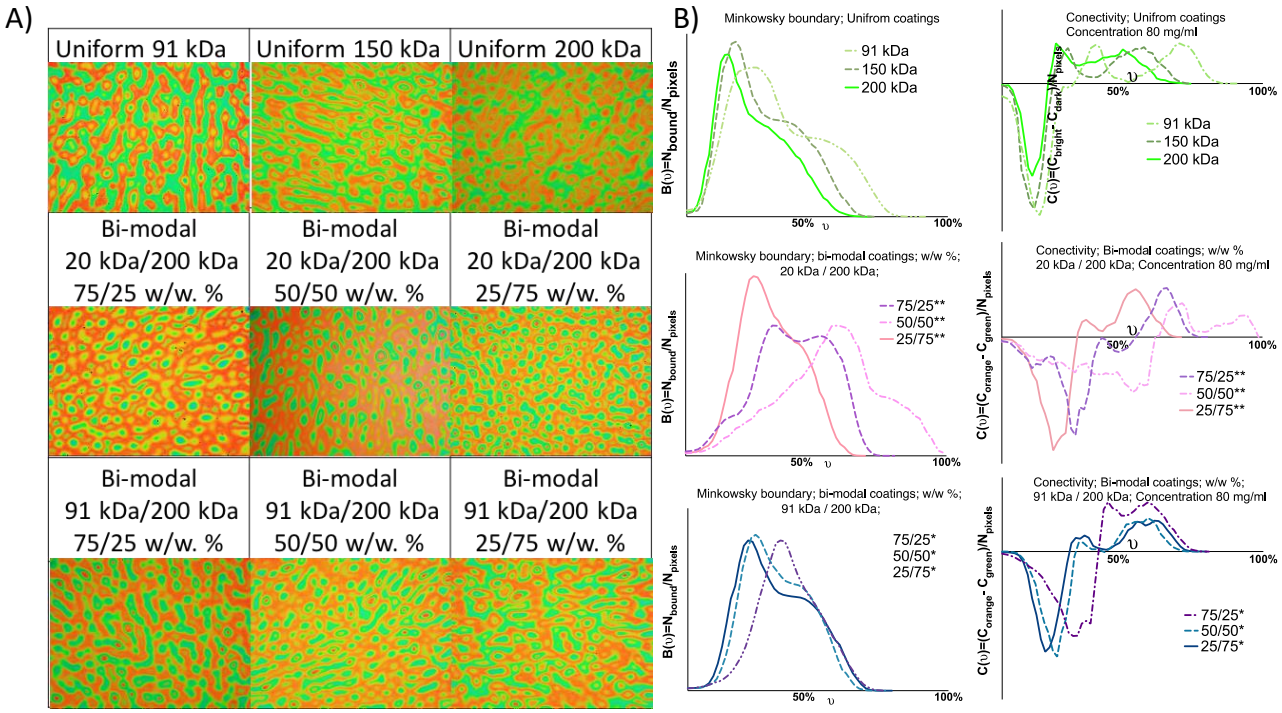

Fig. 7. A - Optical images of coatings spun from 80 mg/ml. The B- Minkowski boundary $B(\nu)$ and connectivity $C(\nu)$, of the coatings spun from 80 mg/ml, where ν represents the threshold for the image binarization, N_{bound} is the number of pixels bounded between bright and light picture areas at a given threshold, N_{pixels} is the total number of pixels, C_{orange} is a total number of orange pixels at a given threshold, C_{green} is the total number of green pixels at a given threshold.

3.4 Investigation of coatings phase composition by means of AFM Force Spectroscopy

AFM Force Spectroscopy method allows to visualize and quantify surface areas differing in mechanical properties.(67) The coatings spun from the solutions with the concentration of 80 mg/ml were studied. By averaging the values from the obtained maps, the resulting elastic modulus of the coatings was calculated (Fig. 8).

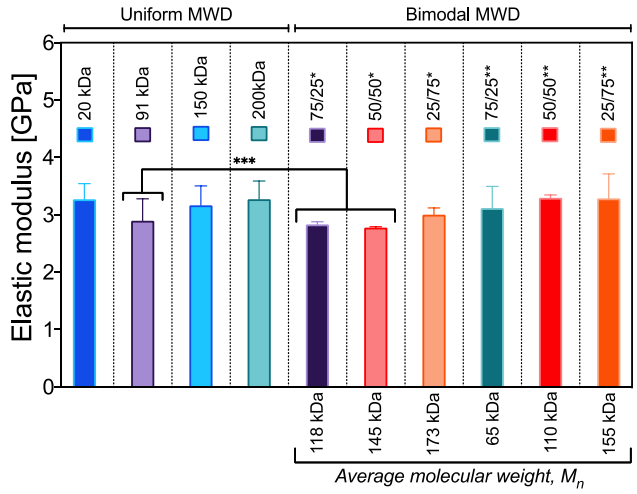

Fig. 8. Average elastic modulus obtained based on the FS method for coatings made from the solution of 80 mg/ml. Uniform – coatings were made from homogeneous solutions; Bimodal – coatings made from solutions with bimodal MWD; * - Blends of 91 kDa and 200 kDa polystyrene; ** - blend of 20 kDa and 200 kDa polystyrene; x/x – w/w% ratio of blended homogeneous polystyrenes. $[M_n] = f_1 M_{w1} + f_2 M_{w2}$, where f w/w % ratio of polymers. *** - means are significantly different (one-way ANOVA, $p < 0.05$).

The obtained results are similar to those found in the literature.(68) The uniform 91 kDa coating and the 75/25 and 50/50 blends of 91 kDa and 200 kDa had significantly lower elastic modulus than the rest of the tested groups. The dependence between the molecular weight and the elastic modulus of polymer has been repeatedly proven.(69,70) However, we have not found significant differences between other groups than those mentioned. In our investigation the

414 uniform 20 kDa coating had similar elastic modulus as the 200 kDa coating. This could have
415 happened due to the influence of the substrate, as the 20 kDa coating was the thinnest. We have
416 performed linear regression test (SI, *Force Spectroscopy*, Fig. S4) between the thickness of the
417 80 mg/ml coatings and the elastic modulus which proved no relationship between the thickness
418 of the coatings and the elastic modulus, while the 20 kDa coating was an outlier (SI, *Force*
419 *Spectroscopy*, Table 14).
420 Interestingly, it was possible to record local differences of the coating surface stiffness (Fig. 9).
421 The maps were gathered for bimodal coatings. White spinodal-like areas are characterized by
422 higher stiffness. The differences are more clearly visible in case of 90 kDa and 200 kDa blends,
423 in agreement with Fig. 8.
424

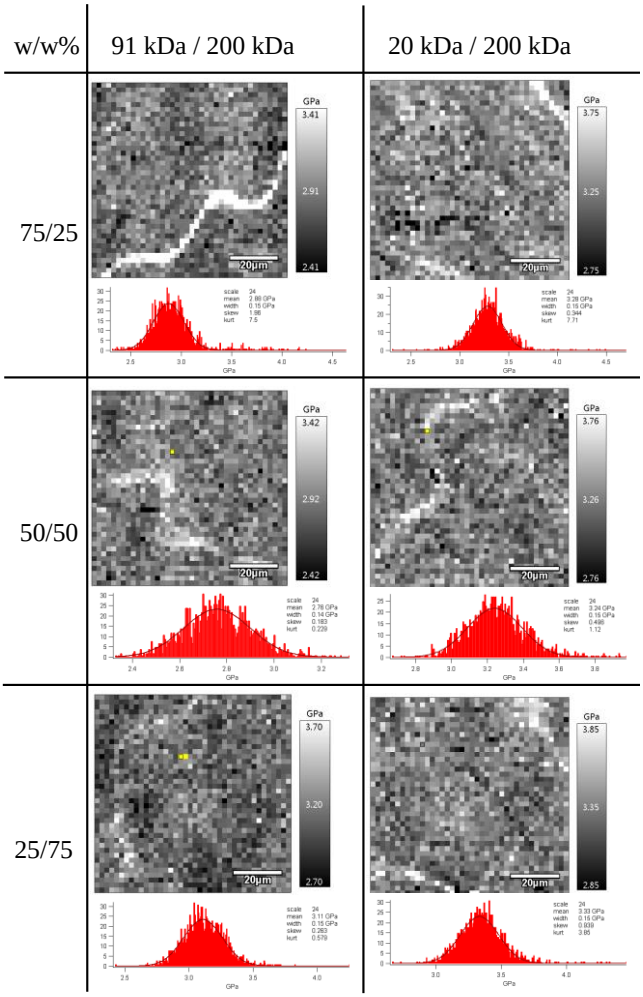

425

Fig. 9. Force Spectroscopy maps of bimodal MWD coatings. The grey scale shows the stiffness – the white color corresponds to the highest stiffness. The gray scale range is ± 1 GPa.

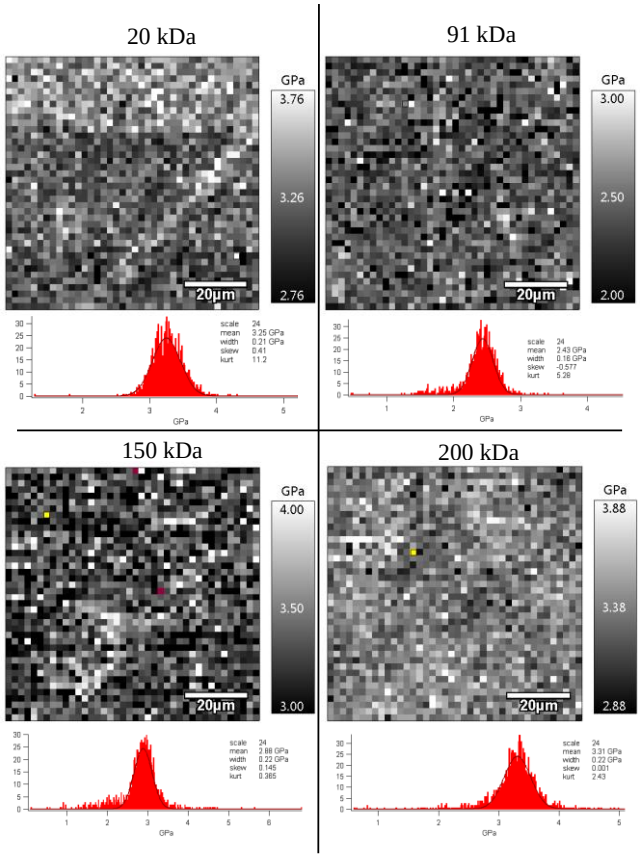

Fig. 10. Force Spectroscopy maps of coatings with uniform MWD. The grey scale shows the stiffness – the white color corresponds to the highest stiffness. The gray scale range is ± 1 GPa.

For comparison, Fig. 10 illustrates the FS maps of the uniform coatings. We have analyzed the skewness of the elastic modulus distribution of the maps (SI, *Force Spectroscopy*, Table S15). The skewness in case of uniform coatings was significantly lower ($p < 0.05$) than in case of the bimodal coatings (Fig. 11). The distribution of the elastic modulus of the uniform coatings was more homogeneous.

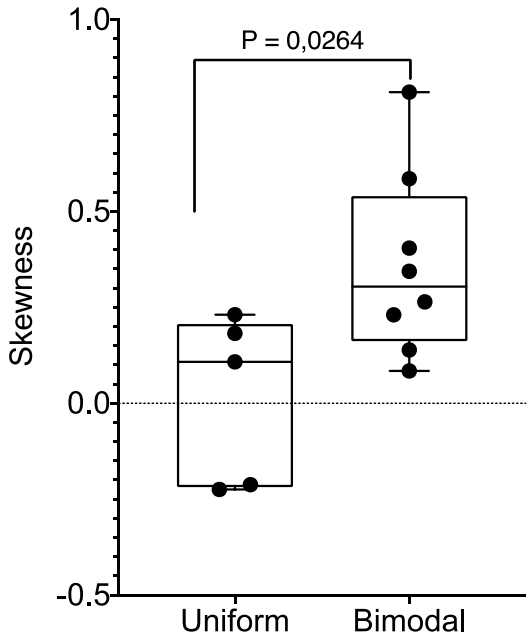

Fig 11. Skewness of the elastic modulus data sets. Uniform – grouped means representing skewness of histograms of uniform coatings elastic modulus. Bimodal – grouped means representing skewness of histograms of all kinds of bimodal blends elastic modulus. The means of these two groups are significantly different ($p < 0.05$).

3.5 Solubility of polystyrenes in respect to the molecular weight distribution

The aforementioned, found by FS, phase segregation could be explained by solubility investigation. It was shown that viscosity of the polymeric solution can be utilized by application of the Mangaraj method to retract several polymer - solvent parameters, i.e. the Flory interaction parameter.(71) We utilized the Mangaraj equation (eq.4) in order to investigate the miscibility gap between the lower and the higher molecular weight polystyrenes. (72)

$$\ln\left(\frac{\eta}{\eta_{max}}\right) = -(\delta_s - \delta_{eff})^2. \quad (4)$$

The effective miscibility parameter δ_{eff} was calculated with respect to a solution of 200 kDa with concentration of 80 mg/ml which had the highest viscosity among the tested solutions (η_{max}). The parameter of the solvent δ_s was set to be 19 $MPa^{0.5}$, which is a typical value for MEK.

In fact, the miscibility gap between low and high molecular weight polystyrene can be derived based on the viscosity of PS blends. Furthermore, the miscibility gap decreases accordingly to the low molecular weight fraction. Here, δ_{eff} is the effective Hildebrand miscibility parameter calculated based on the intrinsic viscosity $[\eta]$. In case of the 20 mg/ml concentration, all the solutions are present on the same linear trend with the lowest δ_{eff} for the highest molecular weight. It should be noted that, with concentration increase, the trends for 20 kDa / 200 kDa solutions (brown squares), 91 kDa / 200 kDa solutions (purple triangles) and the uniform solutions (blue circles) become divergent at low molecular weights, with their trends being coincidental at 200 kDa.

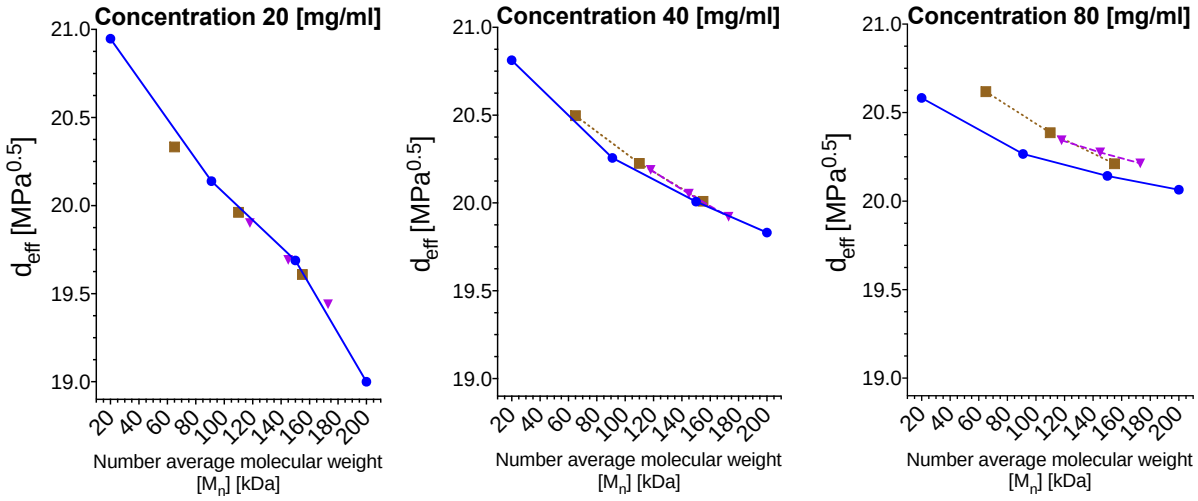

Fig. 12. The effective miscibility parameter δ_{eff} of the polystyrenes in MEK with bimodal and uniform distributions for two kinds of bimodal distributions: 20 kDa / 200 kDa – brown squares and 91 kDa / 200 kDa – purple triangles; the blue circles represent data for polystyrenes with the uniform distributions. $[M_n] = f_1 M_{w1} + f_2 M_{w2}$, where f w/w % ratio of polymers.

3.5 Self-assembly due to phase segregation and water condensation

As a follow-up, we have utilized the humidity in order to take advantage from the phase segregation observed above. The viscosity and solubility investigations pointed to

concentration of 80 mg/ml in order to obtain the most pronounce effect. It is well established method to use the solvent evaporation driven water condensation on the surface of the liquid film to cause ruptures in the film. Water droplets immerse in films and consequently at a higher water concentration this may lead to gaps in the films. After the droplets evaporated, they left cavities inside the film. The condensing water force the film to dewet and retreat from SiO_2. The tested relative humidity Rh values were 45%, 55%, 75%. Fig. 13 A shows images of coatings composed of uniform polystyrenes, Fig. 13 B presents images of coatings prepared from 91 kDa and 200 kDa blends and Fig. 13 C presents images of coatings prepared from 20 kDa and 200 kDa blends. Each column is marked below the PDI value of the mixture and each row corresponds to one of the Rh values. Optical microscope images show larger area of the coatings and are presented in the Supplementary Information, Fig. S6 – S8.

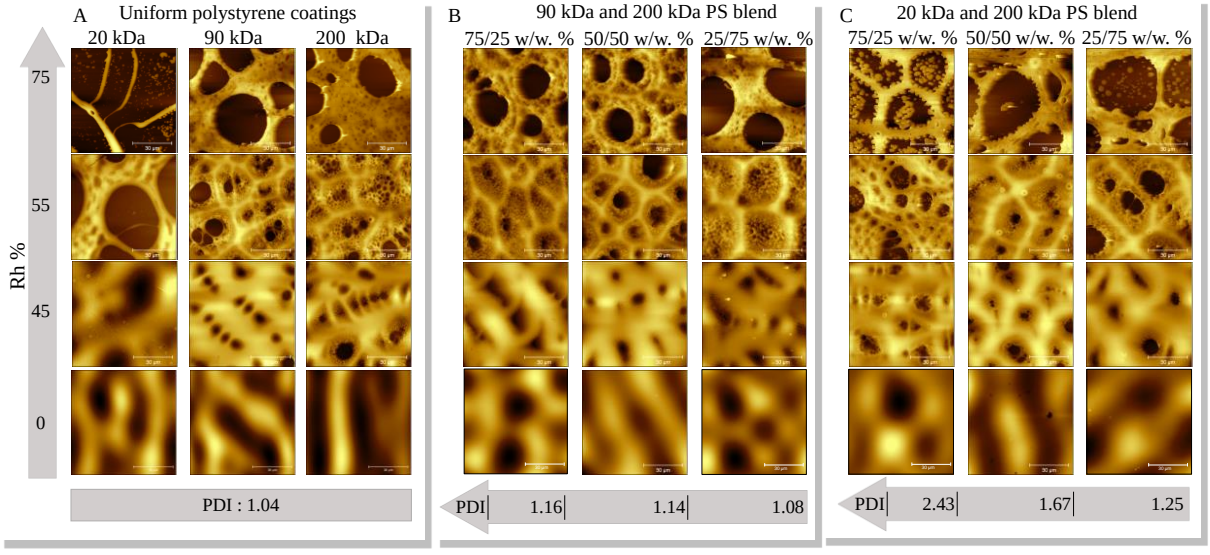

Fig. 13. Morphology of coatings with bimodal MWD spun under different humidity conditions, the solution concentration C was 80 mg/ml. The z-scale was chosen for the best representation of the coating's morphology. A – uniform coatings; B – 20 kDa and 200 kDa blends; C – 91 kDa and 200 kDa blends.

We have observed that the smaller cavities (breath figures) formed around the larger cavities caused by dewetting related polymeric film ruptures. The structure which resembles the honeycomb also occurred. Such patterns are often associated with the Bernardo-Marangoni convention flowing inside a solidifying polymer film. (73,74) The Bernardo-Marangoni's convective flow occurs at a gradient of the surface tension and the evaporation rate. Such gradient may occur due to the aforementioned phase morphology of coatings prepared from bi-modal blends. For Rh 55% the honeycomb-like morphology is found for all of the coatings, except the uniform 20 kDa coating. The proposed process of formation of such complex morphology is presented in Fig. 14.

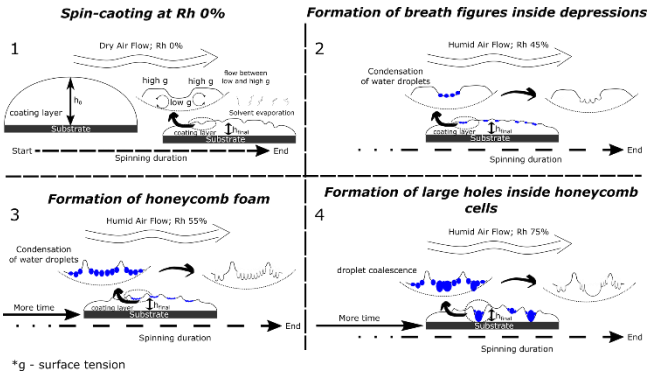

Fig. 14. The chart illustrates the evolution of the morphology of coatings under the influence of the flow of humid air. 1 – Spin-coating in dry conditions, convective flow causes surface roughening. 2 – Condensation of water droplets if the humidity is Rh 45% results in formation of breath figures. 3 – The Marangoni convection and more vapor condensation leads to a honeycomb morphology. 4 – Coalescence of water droplets leads to brakeage of the coating and formation of large pores inside the honeycomb cells.

Notably, the uniform coatings have lost their honeycomb morphologies, when humidity Rh 75% was used. The bimodal coating of 91 kDa and 200 kDa, 25/75 w/w% also did not retain the honeycomb morphology. It should be noted that this kind of coating was the most similar

512 to the uniform coatings during optical imaging and force spectroscopy. Radially averaged
513 Power Spectra Density analysis (SI, Fig. S9) of averaged 4 images depicts the differences
514 between the 75/25, 50/50 and 25/75 w/w% 20 kDa and 200 kDa coatings.
515 Interestingly, the coatings prepared from 20 kDa and 200 kDa bimodal blends at Rh 75% had
516 polymeric pillars inside the large holes. It was found that a certain phase in the polymer film
517 was segregated into structures resembling pillars. An onset of such structures can be observed
518 also in case of coatings prepared in Rh 55%, but the length of the process in this case was too
519 short for full pillar formation. The fraction of the pillars decreased with the increase of 200 kDa
520 contribution. Thus, it can be concluded that the pillars are made of the lower molecular weight
521 fraction. Additionally, we have tested the formation of the micropillars when a short spin-
522 coating time was used (0.5s and 1s). These images are presented in Fig. S15 in SI. The phase
523 segregation was already seen, though, the pillars were not well formed. These results would
524 confirm the reflectometry experiment, which indicated, that the phase separation could happen
525 early on during the spin-coating. Nonetheless, the longer spin-coating time is necessary for
526 enough water condensation to induce the pillar formation.
527 Apparently, as the polymer film receded from the substrate surface, segregation into fractions
528 of varying weight occurred which led to formation of these structures. It was assumed that the
529 pillars are made of the lighter and less viscous fraction. Seemingly, the heavier polymer
530 fraction, more viscous and more entangled reinforced the honeycomb cells borders.
531 Phase segregation was captured by the AFM image (Fig. 15 a - c). The black rectangle indicates
532 the area that differed in terms of deflection signal and phase contrast. It was observed that
533 between this area and the rest of the film was separated by cracks. The water condensation of
534 forced the liquid PS film to dewet from the SiO_2. The direction of dewetting is marked by black
535 arrows. The low molecular weight segregated and separated from the main of the film part of

the film and formed pillars. The proposed mechanism of pillar formation is depicted in Fig 15 d.

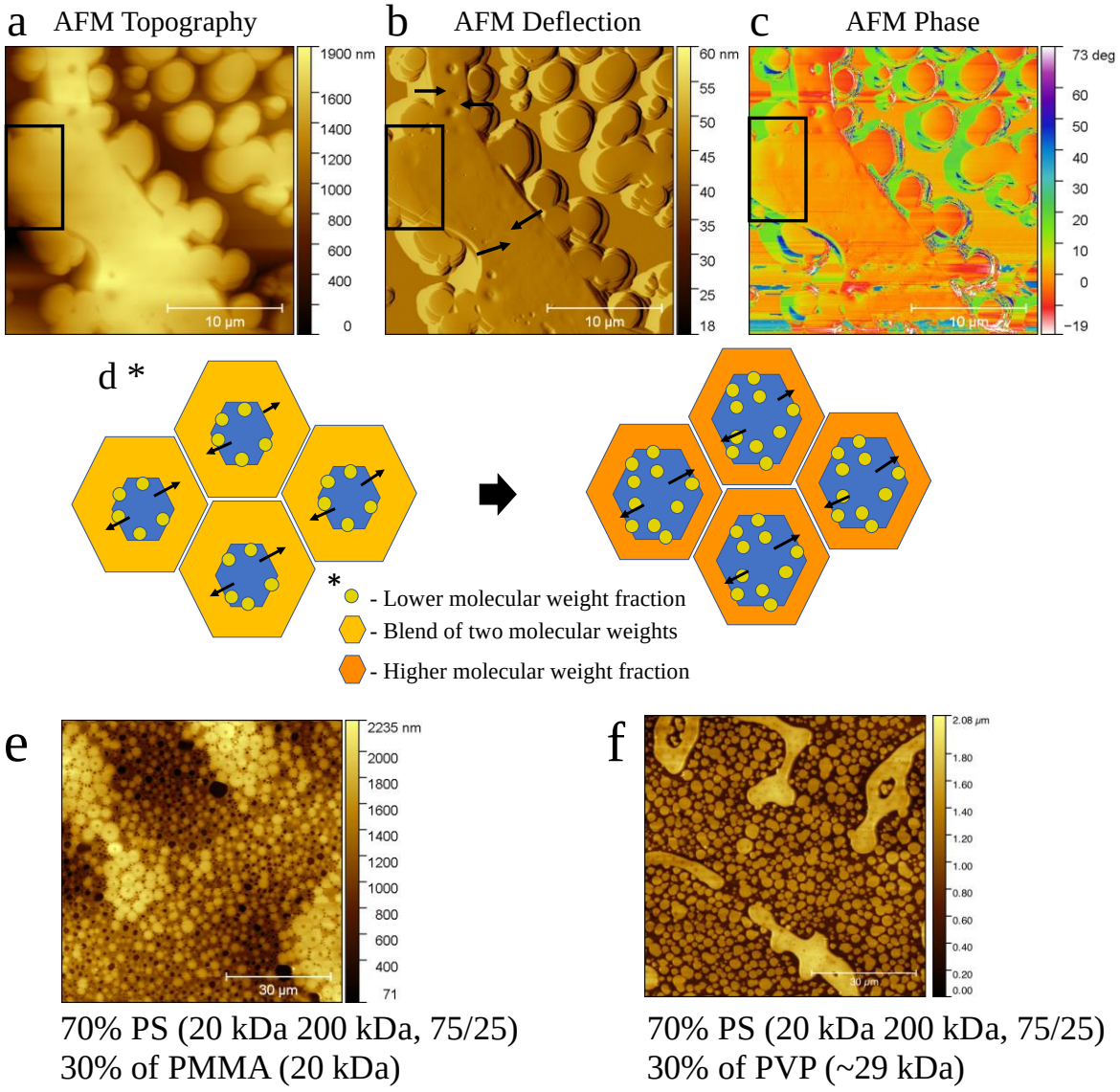

Fig. 15. AFM picture of 20 kDa and 200 kDa 75/25 w/w% blend spun at Rh 75%, the same region is shown in form of a - topography, b - AFM deflection and c - AFM phase images. Black arrows mark the direction of dewetting; d – schematic illustration depicting proposed pillar formation mechanism; Convection inside the liquid film led to cells formation, condensation of water led to film rupture (Blue). Subsequently, recess of the film occurred. At the interface between the rupture area and the receding film segregation of lower molecular fraction occurred (Yellow). Later, the borders of the cells from remaining high molecular

546 weight fraction (Orange); e, f – Blends of 70% of PS with bimodal MWD and PMMA or PVP,
547 respectively.
548 As was mentioned, the polystyrenes used were unmodified standard grade polymers. The
549 unchanged chemical composition of the coatings was confirmed by FTIR spectroscopy (SI Fig.
550 S10 – S12). The recognized functional groups were CH_3, CH_2, and phenyl groups. All of these
551 groups are hydrophobic and were the driving force behind the dewetting process under high
552 humidity conditions. These argument was further reinforced by the Free Surface Energy (SEF)
553 measurement (SI Fig. S13 – S14). The SEF of 20 kDa coating was slightly higher than the 200
554 kDa coating and in consequence lead to higher affinity to the hydrophilic SiO_2 substrate of the
555 former one.
556 Finally, in order to test if the described process can be extended to the other polymer systems,
557 the blends of bi-modal polystyrene and commercially available PMMA or PVP were prepared
558 and spin-coated. In both cases (Fig. 15e and f), segregation of the polystyrene fractions allowed
559 to obtain bimodal morphology of larger and smaller islands.
560
561 **Conclusions**
562 To summarize, polystyrene solutions either with uniform molecular weight distribution or with
563 bimodal molecular weight distribution were used. The bimodal blends consisted either of 20
564 kDa and 200 kDa or of 91 kDa and 200 kDa molecules and 75/25, 50/50 and 25/75 w/w %
565 ratios of these molecules were applied. The blends were dissolved in methyl ethyl ketone and
566 used for spin-coating.
567 • The viscosity of the solutions with bimodal blend distribution was lower than of the
568 uniform solutions (< 20 mg/ml) but increased rapidly with increase of the concentration.
569 The viscosity parameters were tabulated.

- The viscosity data were applied to determine the solubility parameters of bimodal and uniform polystyrene. It was concluded that if the polydispersity of the mixture is high enough, both components of the polystyrene blend can act as separate species and segregate during spin-coating.
- The evaporation pattern during spin-coating and evaporation rate was characterized for each of the polystyrene blends. It was found that bimodal solutions have period of lowered evaporation rate at around 0.4 s of spin-coating.
- The morphology of the bimodal coatings characterized by Minkowski measures and it was concluded that they differ from the morphology of uniform coatings. These result suggested that the convection flow during spinning in the bimodal solutions is different as compare to the uniform solutions.
- Force Spectroscopy reveled spinodal like features in case of the bimodal coatings. These features were visible in both kinds of bimodal blends, when the ratio was 75 to 25.
- It was concluded that the segregation into low and high molecular fractions occurred.
- As the polystyrene is slightly hydrophobic, while the solvent (methyl ethyl ketone) is slightly hydroscopic, it was concluded that the phase separation can be enhanced by spin-coating in high humidity. Coating in relative humidity of 45%, 55% and 75% was tested. It was found, that for 20 kDa and 200 kda blend, at the highest humidity the polystyrene segregated into pillars formed from the lower molecular weight fraction. The higher molecular weight fraction formed the honeycomb cells. It was concluded that these happed due to the difference in viscosity and free surface energy between the two fractions.

It was shown that these phenomenon can be extended into other polymer systems in order to obtain complex and controlled morphology. It is likely possible to apply the described process to other coatings methods, for example dip coating or inkjet printing.

595

596 **Supporting Information (SI)**

597 Experimental setup depicting the custom build spin-coater with a humidity-controlled chamber
598 and an in-situ reflectometer utilizing stroboscopic effect. Illustration of thickness measurement.
599 Viscosity related coefficients. Optical microscope images. FTIR results. Free Surface Energy
600 results.

601

602 **Author information**

603 Corresponding authors:

604 Maciej Łojkowski, ORCID: 0000-0002-0612-7964, email: 00183042@pw.edu.pl
605 Wojciech Swieszkowski, ORCID: 0000-0003-4216-9974, email:
606 wojciech.swieszkowski@pw.edu.pl.

607

608 The authors declare no competing financial interest.

609

610 **Acknowledgments**

611 This manuscript is a part of Maciej Łojkowski PhD thesis. This work was supported by
612 the National Centre for Research and Developments
613 [STRATEGMED3/306888/3/NCBR/2017]. We are grateful miss Mgr. Donata Kuczyńska-
614 Zemła for help with optical microscopy.

615

616 **Authors contributions:**

617 Conceptualization, M.Ł.; methodology, M.Ł., A.Ch., E.Ch.; investigation, M.Ł., A.Ch., E. Ch.,
618 imaging, M.Ł., A.Ch.; data analysis, M.Ł.; visualization, M.Ł.; writing, M.Ł.; supervision, W.

Ś.; revision of the manuscript, M.Ł., A.Ch., E. Ch., W. Ś; funding acquisition W. Ś. All authors have read and agreed to the published version of the manuscript.

Abbreviations

AFM – atomic force microscopy; bimodal – polymer with two nodes in molecular weight distribution; coating – final polymer coating; CA – Contact Angle; E – elastic modulus; film – liquid film of solution spread on the substrate; FS – force spectroscopy; FTIR – Fourier Transform IR; GPC – Gel permeation chromatography; initial solution – solution ate the start of spin-coating; MEK – Methyl Ethyl Ketone; Mw – molecular weight; [M_w] – Weight average molecular weight; [M_n] – Number average molecular weight; MWD – molecular weight distribution; PDI – Polydispersity index; PTF – Polymer thin film; PS – Polystyrene; Rh% - relative humidity in %; RMS – root mean square roughness; Uniform – polymer with one node in molecular weight distribution.

References

1. Kumar M, Bhardwaj R. Wetting characteristics of Colocasia esculenta (Taro) leaf and a bioinspired surface thereof. Sci Rep. 2020;10(1):1–15.
2. He R, Xiao J, Zhang M, Zhang Z, Zhang W, Cao Y, et al. Artificial honeycomb-inspired TiO2 nanorod arrays with tunable nano/micro interfaces for improving poly(dimethylsiloxane) surface hydrophobicity. J Mater Sci. 2016;51(6):2935–41.
3. Jahed Z, Shahsavan H, Verma MS, Rogowski JL, Seo BB, Zhao B, et al. Bacterial Networks on Hydrophobic Micropillars. ACS Nano. 2017;11(1):675–83.
4. Liu X, Liu R, Cao B, Ye K, Li S, Gu Y, et al. Subcellular cell geometry on micropillars regulates stem cell differentiation. Biomaterials [Internet]. 2016;111:27–39. Available from: http://dx.doi.org/10.1016/j.biomaterials.2016.09.023

5. Walheim S, Böltau M, Mlynek J, Krausch G, Steiner U. Structure Formation via Polymer Demixing in Spin-Cast Films. Macromolecules [Internet]. 1997 Aug 1;30(17):4995–5003. Available from: https://doi.org/10.1021/ma9619288
6. Daly R, Sader JE, Boland JJ. The dominant role of the solvent–water interface in water droplet templating of polymers. Soft Matter [Internet]. 2013;9(33):7960. Available from: http://xlink.rsc.org/?DOI=c3sm51452h
7. Khikhlovskyi V, Wang R, van Breemen AJJM, Gelinck GH, Janssen RAJ, Kemerink M. Nanoscale Organic Ferroelectric Resistive Switches. J Phys Chem C [Internet]. 2014 Feb 13;118(6):3305–12. Available from: https://pubs.acs.org/doi/10.1021/jp409757m
8. D'Andrade BW, Forrest SR. White Organic Light-Emitting Devices for Solid-State Lighting. Adv Mater [Internet]. 2004 Sep 16;16(18):1585–95. Available from: http://doi.wiley.com/10.1002/adma.200400684
9. Yabu H. Fabrication of honeycomb films by the breath figure technique and their applications. Sci Technol Adv Mater [Internet]. 2018;19(1):802–22. Available from: https://doi.org/10.1080/14686996.2018.1528478
10. Wu D, Xu F, Sun B, Fu R, He H, Matyjaszewski K. Design and Preparation of Porous Polymers. Chem Rev [Internet]. 2012 Jul 11;112(7):3959–4015. Available from: https://pubs.acs.org/doi/10.1021/cr200440z
11. Karagkiozaki V, Vavoulidis E, Karagiannidis PG, Gioti M, Fatouros DG, Vizirianakis IS, et al. Development of a nanoporous and multilayer drug-delivery platform for medical implants. Int J Nanomedicine. 2012;7(October):5327–38.
12. Calejo MT, Ilmarinen T, Skottman H, Kellomäki M. Breath figures in tissue engineering and drug delivery: State-of-the-art and future perspectives. Vol. 66, Acta Biomaterialia. 2018.

669 13. Vendra VK, Wu L, Krishnan S. Polymer Thin Films for Biomedical Applications. In:
670 Nanotechnologies for the Life Sciences [Internet]. Weinheim, Germany: Wiley-VCH
671 Verlag GmbH & Co. KGaA; 2011. Available from:
672 http://doi.wiley.com/10.1002/9783527610419.ntls0179
673 14. Griesser HJ. Thin Film Coatings for Biomaterials and Biomedical Applications, 1st
674 Edition. 2016. 310 p.
675 15. Łojkowski M, Walheim S, Jokubauskas P, Schimmel T, Święszkowski W. Tuning the
676 wettability of a thin polymer film by gradually changing the geometry of nanoscale
677 pore edges. Langmuir [Internet]. 2019;35(17):5987–96. Available from:
678 https://doi.org/10.1021/acs.langmuir.9b00467
679 16. Plawsky JL, Kim JK, Schubert EF. Engineered nanoporous and nanostructured films.
680 Mater Today [Internet]. 2009;12(6):36–45. Available from:
681 http://dx.doi.org/10.1016/S1369-7021(09)70179-8
682 17. Bormashenko E. Breath-figure self-assembly, a versatile method of manufacturing
683 membranes and porous structures: Physical, chemical and technological aspects.
684 Membranes (Basel). 2017;7(3).
685 18. van Franeker JJ, Westhoff D, Turbiez M, Wienk MM, Schmidt V, Janssen RAJ.
686 Controlling the Dominant Length Scale of Liquid-Liquid Phase Separation in Spin-
687 coated Organic Semiconductor Films. Adv Funct Mater [Internet]. 2015
688 Feb;25(6):855–63. Available from: http://doi.wiley.com/10.1002/adfm.201403392
689 19. Schaefer C, Michels JJ, van der Schoot P. Structuring of Thin-Film Polymer Mixtures
690 upon Solvent Evaporation. Macromolecules [Internet]. 2016 Sep 27;49(18):6858–70.
691 Available from: https://pubs.acs.org/doi/10.1021/acs.macromol.6b00537
692 20. Ebbens S, Hodgkinson R, Parnell AJ, Dunbar A, Martin SJ, Topham PD, et al. In Situ
693 Imaging and Height Reconstruction of Phase Separation Processes in Polymer Blends

during Spin Coating. ACS Nano [Internet]. 2011 Jun 28;5(6):5124–31. Available from: https://pubs.acs.org/doi/10.1021/nn201210e

21. Danglad-Flores J, Eickelmann S, Riegler H. Deposition of polymer films by spin casting: A quantitative analysis. Chem Eng Sci [Internet]. 2018 Apr;179:257–64. Available from: https://linkinghub.elsevier.com/retrieve/pii/S0009250918300125

22. Daly R, Sader JE, Boland JJ. Taming Self-Organization Dynamics to Dramatically Control Porous Architectures. ACS Nano [Internet]. 2016 Mar 22;10(3):3087–92. Available from: https://pubs.acs.org/doi/10.1021/acsnano.5b06082

23. Müller-Buschbaum P, Gutmann JS, Wolkenhauer M, Kraus J, Stamm M, Smilgies D, et al. Solvent-Induced Surface Morphology of Thin Polymer Films. Macromolecules [Internet]. 2001 Feb;34(5):1369–75. Available from: https://pubs.acs.org/doi/10.1021/ma0009193

24. Bornside DE. Spin Coating of a PMMA/Chlorobenzene Solution. J Electrochem Soc [Internet]. 1991;138(1):317. Available from: https://iopscience.iop.org/article/10.1149/1.2085563

25. Wodo O, Ganapathysubramanian B. Modeling morphology evolution during solvent-based fabrication of organic solar cells. Comput Mater Sci [Internet]. 2012;55:113–26. Available from: http://dx.doi.org/10.1016/j.commatsci.2011.12.012

26. Huang C, Förste A, Walheim S, Schimmel T. Polymer blend lithography for metal films: Large-area patterning with over 1 billion holes/inch2. Beilstein J Nanotechnol. 2015;6(1):1205–11.

27. Wu BH, Zhong QZ, Xu ZK, Wan LS. Effects of molecular weight distribution on the self-assembly of end-functionalized polystyrenes. Polym Chem. 2017;8(29):4290–8.

28. Jiang H, Zhang L, Qin J, Zhang W, Cheng Z, Zhu X. Producing bimodal molecular weight distribution polymers through facile one-pot/one-step RAFT polymerization. J

719 Polym Sci Part A Polym Chem. 2012;50(19):4103–9.
720 29. Whitfield R, Parkatzidis K, Truong NP, Junkers T, Anastasaki A. Tailoring Polymer
721 Dispersity by RAFT Polymerization: A Versatile Approach. Chem [Internet]. 2020
722 Jun;6(6):1340–52. Available from:
723 https://linkinghub.elsevier.com/retrieve/pii/S2451929420301923
724 30. Tanaka K, Takahara A, Kajiyama T. Effect of Polydispersity on Surface Molecular
725 Motion of Polystyrene Films. Macromolecules [Internet]. 1997 Oct;30(21):6626–32.
726 Available from: https://pubs.acs.org/doi/10.1021/ma970057e
727 31. Zabusky HH, Heitmiller RF. Properties of high density polyethylenes with bimodal
728 molecular weight distribution. Polym Eng Sci. 1964;4(1):17–21.
729 32. Heitmiller RF, Naar RZ, Zabusky HH. Effect of homogeneity on viscosity in capillary
730 extrusion of polyethylene. J Appl Polym Sci [Internet]. 1964 Mar;8(2):873–80.
731 Available from: http://doi.wiley.com/10.1002/app.1964.070080226
732 33. Koningsveld R, Chermin HAG, Gordon M. Liquid─liquid phase separation in
733 multicomponent polymer solutions - VIII. Stability limits and consolute states in quasi-
734 ternary mixtures. Proc R Soc London A Math Phys Sci [Internet]. 1970 Oct
735 27;319(1538):331–49. Available from:
736 https://royalsocietypublishing.org/doi/10.1098/rspa.1970.0182
737 34. Zeman L, Patterson D. Effect of the Solvent on Polymer Incompatibility in Solution.
738 Macromolecules [Internet]. 1972 Jul;5(4):513–6. Available from:
739 https://pubs.acs.org/doi/abs/10.1021/ma60028a030
740 35. Shultz AR, Flory PJ. Phase Equilibria in Polymer—Solvent Systems1,2. J Am Chem
741 Soc [Internet]. 1952 Oct 1;74(19):4760–7. Available from:
742 https://doi.org/10.1021/ja01139a010
743 36. Harris EK. Effect of blending on the rheological properties of polystyrene. J Appl

744 Polym Sci [Internet]. 1973 Jun;17(6):1679–92. Available from:
745 http://doi.wiley.com/10.1002/app.1973.070170604
746 37. Klein J. The Onset of Entangled Behavior in Semidilute and Concentrated Polymer
747 Solutions. Macromolecules [Internet]. 1978 Sep;11(5):852–8. Available from:
748 https://pubs.acs.org/doi/abs/10.1021/ma60065a002
749 38. Hong KM, Noolandi J. Theory of inhomogeneous multicomponent polymer systems.
750 Macromolecules [Internet]. 1981 May;14(3):727–36. Available from:
751 https://pubs.acs.org/doi/abs/10.1021/ma50004a051
752 39. Hariharan A, Kumar SK, Russell TP. A lattice model for the surface segregation of
753 polymer chains due to molecular weight effects. Macromolecules [Internet]. 1990
754 Jul;23(15):3584–92. Available from:
755 https://pubs.acs.org/doi/abs/10.1021/ma00217a009
756 40. Mahmoudi P, Matsen MW. Entropic segregation of short polymers to the surface of a
757 polydisperse melt. Eur Phys J E [Internet]. 2017 Oct 6;40(10):85. Available from:
758 http://link.springer.com/10.1140/epje/i2017-11575-7
759 41. Hill JA, Endres KJ, Mahmoudi P, Matsen MW, Wesdemiotis C, Foster MD. Detection
760 of Surface Enrichment Driven by Molecular Weight Disparity in Virtually
761 Monodisperse Polymers. ACS Macro Lett [Internet]. 2018 Apr 17;7(4):487–92.
762 Available from: https://pubs.acs.org/doi/10.1021/acsmacrolett.7b00993
763 42. Stein GE, Laws TS, Verduzco R. Tailoring the Attraction of Polymers toward Surfaces.
764 Macromolecules [Internet]. 2019 Jul 9;52(13):4787–802. Available from:
765 https://pubs.acs.org/doi/10.1021/acs.macromol.9b00492
766 43. Carlier V, Sclavons M, Jonas AM, Jérôme R, Legras R. Probing Thermoplastic
767 Matrix−Carbon Fiber Interphases. 1. Preferential Segregation of Low Molar Mass
768 Chains to the Interface. Macromolecules [Internet]. 2001 May;34(11):3725–9.

Available from: https://pubs.acs.org/doi/10.1021/ma000404b

44. Suwa J, Kakiage M, Yamanobe T, Komoto T, Uehara H. Molecular Weight Segregation on Surfaces of Polyethylene Blended Films as Estimated from Nanoscratch Tests Using Scanning Probe Microscopy. Langmuir [Internet]. 2007 May;23(11):5882–5. Available from: https://pubs.acs.org/doi/10.1021/la070150o

45. Karim A, Slawecki TM, Kumar SK, Douglas JF, Satija SK, Han CC, et al. Phase-Separation-Induced Surface Patterns in Thin Polymer Blend Films. Macromolecules [Internet]. 1998 Feb;31(3):857–62. Available from: https://pubs.acs.org/doi/10.1021/ma970687g

46. Hoppe H, Heuberger M, Klein J. Self-Similarity and Pattern Selection in the Roughening of Binary Liquid Films. Phys Rev Lett [Internet]. 2001 May 21;86(21):4863–6. Available from: https://link.aps.org/doi/10.1103/PhysRevLett.86.4863

47. Heier J, Kramer EJ, Revesz P, Battistig G, Bates FS. Spinodal Decomposition in a Subsurface Layer of a Polymer Blend Film. Macromolecules [Internet]. 1999 Jun;32(11):3758–65. Available from: https://pubs.acs.org/doi/10.1021/ma981709h

48. Jandt KD, Heier J, Bates FS, Kramer EJ. Transient surface roughening of thin films of phase separating polymer mixtures. Langmuir. 1996;12(15):3716–20.

49. Flory PJ, Höcker H. Thermodynamics of polystyrene solutions. Part 1.—Polystyrene and methyl ethyl ketone. Trans Faraday Soc [Internet]. 1971;67:2258–69. Available from: http://xlink.rsc.org/?DOI=TF9716702258

50. Imre A, Van Hook WA. Liquid-liquid demixing from solutions of polystyrene. 1. A review. 2. Improved correlation with solvent properties. Vol. 25, Journal of Physical and Chemical Reference Data. 1996. p. 637–61.

51. Zgłobicka I, Chlanda A, Woźniak M, Łojkowski M, Szoszkiewicz R, Mazurkiewicz-

Pawlicka M, et al. Microstructure and nanomechanical properties of single stalks from diatom Didymosphenia geminata and their change due to adsorption of selected metal ions. J Phycol. 2017;53(4).

52. Chlanda A, Kijeńska-Gawrońska E, Zdunek J, Swieszkowski W. Internal nanocrystalline structure and stiffness alterations of electrospun polycaprolactone-based mats after six months of in vitro degradation. An atomic force microscopy assay. J Mech Behav Biomed Mater [Internet]. 2020 Jan;101(August 2019):103437. Available from: https://linkinghub.elsevier.com/retrieve/pii/S1751616119305156

53. Sader JE, Borgani R, Gibson CT, Haviland DB, Michael J, Kilpatrick JI, et al. A virtual instrument to standardise the calibration of atomic force microscope cantilevers. Rev Sci Instrum [Internet]. 2016 Sep 1;87(9):093711. Available from: http://dx.doi.org/10.1063/1.4962866

54. Wu KC, You HI. Determination of solid material elastic modulus and surface energy based on JKR contact model. Appl Surf Sci. 2007;253(20):8530–7.

55. Toolan DTW. Straightforward technique for in situ imaging of spin-coated thin films . Opt Eng. 2015;54(2):024109.

56. Toolan DTW, Howse JR. Development of in situ studies of spin coated polymer films. J Mater Chem C. 2013;1(4):603–16.

57. Mokarian-Tabari P, Geoghegan M, Howse JR, Heriot SY, Thompson RL, Jones RAL. Quantitative evaluation of evaporation rate during spin-coating of polymer blend films: Control of film structure through defined-atmosphere solvent-casting. Eur Phys J E. 2010;33(4):283–9.

58. Heriot SY, Jones RAL. An interfacial instability in a transient wetting layer leads to lateral phase separation in thin spin-cast polymer-blend films. Nat Mater. 2005;4(10):782–6.

59. Drelich JW, Boinovich L, Chibowski E, Volpe C Della, Hołysz L, Marmur A, et al. Contact Angles: History of Over 200 Years of Open Questions. Surf Innov [Internet]. 2019;(March):1–25. Available from: https://www.icevirtuallibrary.com/doi/10.1680/jsuin.19.00007

60. Koningsveld R, Staverman AJ. Liquid–liquid phase separation in multicomponent polymer solutions. I. Statement of the problem and description of methods of calculation. J Polym Sci Part A-2 Polym Phys [Internet]. 1968 Feb;6(2):305–23. Available from: http://doi.wiley.com/10.1002/pol.1968.160060201

61. Utracki LA, Wilkie CA. Polymer blends handbook. Polymer Blends Handbook. 2014. 1–2378 p.

62. Ying Q, Chu B. Overlap concentration of macromolecules in solution. Macromolecules [Internet]. 1987 Mar;20(2):362–6. Available from: https://pubs.acs.org/doi/abs/10.1021/ma00168a023

63. Kim JK, Taki K, Nagamine S, Ohshima M. Periodic porous stripe patterning in a polymer blend film induced by phase separation during spin-casting. Langmuir. 2008;24(16):8898–903.

64. Heier J, Kramer EJ, Groenewold J, Fredrickson GH. Kinetics of individual block copolymer island formation and disappearance near an absorbing boundary. Macromolecules. 2000;33(16):6060–7.

65. Coveney S, Clarke N. Pattern formation in polymer blend thin films: Surface roughening couples to phase separation. Phys Rev Lett. 2014;113(21):1–5.

66. Mecke K. Additivity, Convexity, and Beyond: Applications of Minkowski Functionals in Statistical Physics. Stat Phys Spat Stat [Internet]. 2000;111–84. Available from: http://link.springer.com/chapter/10.1007/3-540-45043-2_6

67. Wolf BA. Improvement of polymer solubility: Influence of shear and of pressure. Pure

Appl Chem. 1997;69(5):929–33.

68. Du B, Tsui OKC, Zhang Q, He T. Study of Elastic Modulus and Yield Strength of Polymer Thin Films Using Atomic Force Microscopy. Langmuir [Internet]. 2001 May;17(11):3286–91. Available from: https://pubs.acs.org/doi/10.1021/la001434a

69. Landel RF, Nielsen LE. Mechanical properties of polymers and composites. CRC press; 1993.

70. Torres JM, Stafford CM, Vogt BD. Impact of molecular mass on the elastic modulus of thin polystyrene films. Polymer (Guildf) [Internet]. 2010;51(18):4211–7. Available from: http://dx.doi.org/10.1016/j.polymer.2010.07.003

71. Kok CM, Rudin A. Prediction of Flory–Huggins interaction parameters from intrinsic viscosities. J Appl Polym Sci. 1982;27(2):353–62.

72. Lee SH, Lee SB. The Hildebrand solubility parameters, cohesive energy densities and internal energies of 1-alkyl-3-methylimidazolium-based room temperature ionic liquids. Chem Commun. 2005;(27):3469–71.

73. Bormashenko E, Malkin A, Musin A, Bormashenko Y, Whyman G, Litvak N, et al. Mesoscopic patterning in evaporated polymer solutions: Poly(ethylene glycol) and room-temperature-vulcanized polyorganosilanes/-siloxanes promote formation of honeycomb structures. Macromol Chem Phys. 2008;209(6):567–76.

74. Uchiyama H, Matsui T, Kozuka H. Spontaneous Pattern Formation Induced by Bénard–Marangoni Convection for Sol–Gel-Derived Titania Dip-Coating Films: Effect of Co-solvents with a High Surface Tension and Low Volatility. Langmuir [Internet]. 2015 Nov 17;31(45):12497–504. Available from: https://pubs.acs.org/doi/10.1021/acs.langmuir.5b02929

869 **TOC**

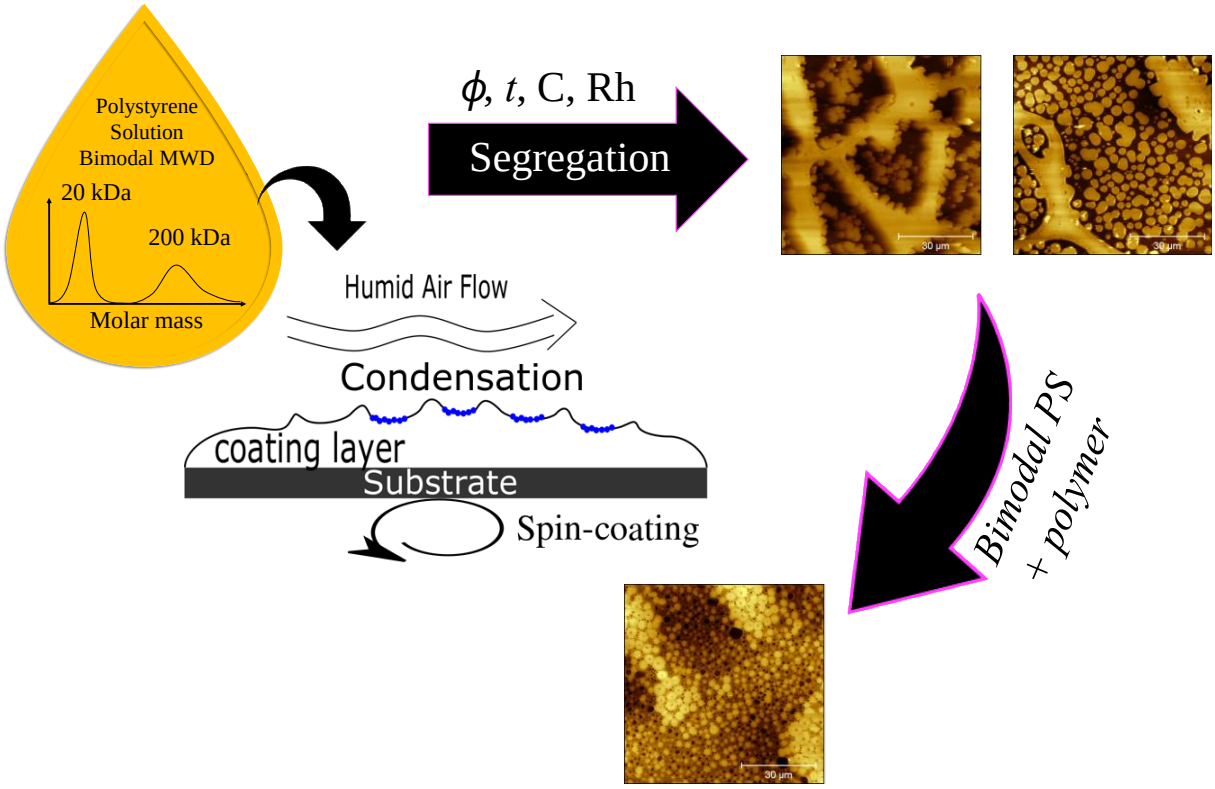

Two kind of PS islands

870